

Lattice and surface effects in the out-of-equilibrium dynamics of the Hubbard modelPatrice André,¹ M. Schiró,² and Michele Fabrizio^{1,3}¹*International School for Advanced Studies (SISSA) and CNR-IOM Democritos, Via Bonomea 265, I-34136 Trieste, Italy*²*Princeton Center for Theoretical Science and Department of Physics, Joseph Henry Laboratories, Princeton University, Princeton, New Jersey 08544, USA*³*The Abdus Salam International Centre for Theoretical Physics (ICTP), P.O. Box 586, I-34014 Trieste, Italy*

(Received 20 February 2012; published 10 May 2012)

We study, by means of the time-dependent Gutzwiller approximation, the out-of-equilibrium dynamics of a half-filled Hubbard-Holstein model of correlated electrons interacting with local phonons. Inspired by pump-probe experiments, where intense light pulses selectively induce optical excitations that trigger a transient out-of-equilibrium dynamics, here we inject energy in the Hubbard bands by a nonequilibrium population of empty and doubly-occupied sites. We first consider the case of a global perturbation, acting over the whole sample, and find evidence of a mean-field dynamical transition where the lattice gets strongly distorted above a certain energy threshold, despite the weak strength of the electron-phonon coupling by comparison with the Hubbard repulsion. Next, we address a slab geometry for a correlated heterostructure and study the relaxation dynamics across the system when the perturbation acts locally on the first layer. While for weak deviations from equilibrium the excited surface is able to relax by transferring its excess energy to the bulk, for large deviations, the excess energy stays instead concentrated in the surface layer. This self-trapping occurs both in the absence as well as in the presence of electron-phonon coupling. Phonons actually enforce the trapping by distorting at the surface.

DOI: [10.1103/PhysRevB.85.205118](https://doi.org/10.1103/PhysRevB.85.205118)

PACS number(s): 71.10.Fd, 71.30.+h, 78.47.-p

I. INTRODUCTION

The transient dynamical behavior of correlated materials optically excited far from equilibrium is currently attracting growing interest due to the impressive advances in time-resolved spectroscopy with femtosecond resolution. By shining the sample with intense ultrafast pulses (pump), one can trigger nonequilibrium transient states, whose physical properties are then recorded by a second pulse arriving at fixed time delay (probe). The unique feature of these experimental techniques is to give access to dynamical information unavailable to conventional time-averaged frequency domain spectroscopies.¹ In addition, when irradiation is sufficiently strong, one can even stabilize transient states with fundamentally different physical properties,² thus paving the way to a complete control of material properties by light.³ As correlated electron systems are often on the verge of a Mott metal-to-insulator transition, this portends the utmost important possibility of optically manipulating their conducting properties on ultrashort time scales.⁴

Motivated by these achievements, the research activity on transient ultrafast dynamics in correlated electronic systems has rapidly grown in recent years.⁵⁻⁹ From a theoretical perspective, one can expect a nontrivial and rich transient dynamical behavior to emerge, reflecting the complex interplay between electrons, phonons, spins, and orbital degrees of freedom that characterizes the phase diagram of these materials. On a more fundamental level, the crucial question concerns whether these experiments could allow to explore novel metastable phases of correlated quantum matter that can only be accessed along nonthermal pathways.

A common wisdom is that the effect of perturbing the system by an ultrashort laser pulse can be qualitatively accounted for by an effective-temperature description.¹⁰⁻¹³ Within this picture, the injected energy would turn first, on

few femtoseconds, into heat for the electron subsystem only. At later times, picoseconds, the electronic heat is gradually transferred to the lattice so that, eventually, the whole system flows to a thermal state at higher temperature than the initial one. Under such a thermodynamic assumption, optical pumping should mimic the role of heating, hence allow accessing, possibly much faster, all phases that are reached upon raising temperature at equilibrium. In the specific case of correlated materials, this entails the possibility of photoinducing metal-to-insulator transitions. Indeed, there exist many examples of Mott insulators that can be driven metallic upon increasing temperature, like, e.g., V_2O_3 (see Ref. 14 and 15) and VO_2 (see Ref. 15), and, vice versa, metals that turn Mott insulating upon heating, like the same V_2O_3 (see Ref. 14 and 15) at higher temperatures, or like doped manganites.¹⁶

However, a deeper thought of what is known about correlated systems in equilibrium already raises questions on this point of view. Indeed, according to this picture, one must conclude that energy pumping, assumed to be equivalent to temperature raising, should make a metal less metallic and a band insulator less insulating. It is believed¹⁷ that a correlated metal near a Mott transition actually shares properties of both metals and insulators; itinerant quasiparticles narrowly centered around the chemical potential coexisting with incoherent atomiclike high-energy excitations, the so-called Hubbard bands. If intense light exposure is the same as heating, and since the light is selective via its frequency and polarization, then one could envisage the quasiparticles or else the Hubbard bands being heated first, which would correspond, respectively, to conductivity decrease or increase. Such a nonmonotonous behavior would, however, contrast the effect of raising temperature at equilibrium, which is supposed to always lower conductivity.¹⁷ The above observation thus challenges the picture of pump-probe experiments as

effective thermodynamic perturbations. Indeed, while temperature excites the system incoherently by making high-energy states contribute with their own Boltzmann factor and density, light is able to selectively create specific excitations. This property may lead to substantial differences from thermal effects, especially, in the case of correlated metals, where the same conduction electrons are characterized by well distinct energy scales, some corresponding to itinerant and other to more localized excitations.

A different perspective, pointing toward an intrinsic kinetic nature of these experimental settings, is offered by the intense research activity around the non equilibrium dynamics of closed isolated many-body systems, which has recently attracted lot of interest in the different context of cold atoms trapped in optical lattices.¹⁸ In this respect, it is by now well established that, when driven out of equilibrium by intense sudden perturbations, strongly correlated systems can be trapped into long-lived metastable states that differ qualitatively from their equilibrium counterpart. An example along this line is provided by the single-band Hubbard model, likely the simplest model to describe strong-correlation physics. Different theoretical approaches^{19–21} have shown, for example, that a sudden increase of the Hubbard repulsion drives the system into a long-lived metastable state which, although highly excited, shows intrinsic features of a zero-temperature metallic state, rather than incoherent finite-temperature effects as one would have guessed by thermodynamic arguments. Seemingly, suddenly switching on a large Hubbard repulsion stabilizes metastable phases rich of energetically unfavorable doubly occupied sites, which are kinetically blocked²⁰ and unable to decay²² or even to coherently propagate.²³ A qualitative picture of the crossovers or genuine dynamical transitions between different metastable states in the Hubbard model driven by sudden quantum quenches has been recently obtained using a time-dependent extension of the Gutzwiller approximation (t-GA).^{24,25} While missing important quantum fluctuations, which are crucial for the long-time dynamics, this approximate scheme has been shown to capture important qualitative features of the intermediate time evolution, which is actually of interest in the description of the pump-probe dynamics.

In this work, we aim to elaborate further on this out of equilibrium perspective by including additional ingredients that might play an important role in modeling pump-probe experiments on actual correlated materials. Firstly, we add phonons to the half-filled single-band Hubbard model and study the transient dynamics induced by a sudden perturbation. It is worth noticing that lattice vibrations play a crucial role in actual experiments by triggering selective perturbation for the electronic subsystem,²⁶ and their role in ultrafast pump probe experiments is a subject of current experimental interest.^{27–29} Here, we consider Einstein phonons coupled to the local charge and study the dynamics of the resulting Hubbard-Holstein model using a suitable extension of t-GA. Although extremely simplified, this model represents a first attempt to figure out how highly excited electrons succeed in transferring their excess energy to the lattice. Results reveal, akin to the pure Hubbard model, the existence of a metastable state for high enough excitation, where phonons get strongly displaced in spite the large Coulomb repulsion and in striking contrast to what one would have guessed in equilibrium.

A second important ingredient that we add to the description builds on the observation recently reported in a number of theoretical investigations that nonthermal metastable states are extremely sensitive to spatial fluctuations and prone to spontaneous generation of inhomogeneities,^{23,30} which could play a crucial role in the dynamics, in particular, around dynamical transition points.^{25,31} To investigate this issue, we consider the same Hubbard-Holstein model at half-filling but now in a slab geometry that lacks translational symmetry, modeling ultrafast dynamics in correlated heterostructures.²⁹ We assume that, initially, only the surface layer is driven out of equilibrium and study by t-GA how the excess energy is redistributed inside the bulk. Remarkably, if the energy initially stored on the surface exceeds a critical threshold, it remains trapped on the uppermost layers. Concomitantly, the phonons distort at the surface, providing a further trapping potential. This result demonstrates not only the importance of inhomogeneities, but also suggests that, under specific circumstances, the lattice might not provide a dissipative bath to speed up relaxation, but rather play the opposite game to slow down thermalization.

The paper is organized as follows. In Sec. II, we introduce the model and an out-of-equilibrium version of the Gutzwiller approximation that may cope with the electron-phonon coupling. In Sec. II A, we show that the method is equivalent to the mean-field approximation applied to a model of free electrons coupled to phonons and Ising spins. In Sec. III, we move to discuss the results for two different cases. First, in Sec. III A, we study the time evolution when the whole bulk is suddenly driven out of equilibrium. Next, in Sec. III B, we consider the situation in which an external pulse only excites the surface layer, and study if and how the surface can relax by transferring energy to the bulk. Finally, Sec. IV is devoted to concluding remarks.

II. THE MODEL AND THE GUTZWILLER APPROXIMATION

We consider a half-filled Hubbard-Holstein model described by the Hamiltonian

$$H = -t \sum_{(ij)\sigma} (c_{i\sigma}^\dagger c_{j\sigma} + \text{H.c.}) + \frac{U}{2} \sum_i (n_i - 1)^2 + \frac{\omega}{2} \sum_i (p_i^2 + x_i^2) - g \sum_i x_i (n_i - 1),$$

where $c_{i\sigma}^\dagger$ ($c_{i\sigma}$) creates (annihilates) an electron with spin σ at site i , x_i is the phonon displacement at that site, and p_i its conjugate variable. The hopping is restricted to nearest neighbors and n_i is the electron number operator. We note that Eq. (1) is invariant under particle-hole transformation provided $x_i \rightarrow -x_i$.

In the following, we study the unitary dynamics induced by the Hamiltonian (1) using the Gutzwiller variational scheme introduced at equilibrium by Barone *et al.*^{32,33} and extended to the time-dependent case following Ref. 24. It is worth mentioning that at equilibrium the method is able to reproduce even quantitatively the exact results of DMFT, as discussed extensively in Ref. 33, which is important in view of the present extension to the out-of-equilibrium dynamics.

We emphasize at this point that, in real experiments, the light pulse couples via the vector potential to the electronic degrees of freedom. While, in principle, the variational description could be extended to include this feature, here we assume for the sake of simplicity that the effect of the pump is mainly to induce an initial nonequilibrium distribution of electronic degrees of freedom, whose dynamics is then driven by the Hubbard-Holstein Hamiltonian. Furthermore, while in real experimental settings, the system is always in contact with a thermostat that eventually allows the injected energy to flow away, here we assume the whole system made by electrons and lattice to be isolated. While in different contexts, e.g., when current-carrying stationary states driven by static electric fields are present, this assumption may be highly questionable, here we stress that our focus concerns the transient relaxation dynamics on time scales of electronic and phononic degrees of freedom. As the coupling with the environment is typically very weak, we do not believe that this assumption can qualitatively change the physical picture that we will draw.

With these assumptions on the theoretical side, we now introduce our time-dependent variational wave function for the dynamics of the Hubbard-Holstein model (1). Specifically, we write

$$|\Psi(t)\rangle = \prod_i \mathcal{P}_i(x_i, t) |\Psi_0(t)\rangle, \quad (1)$$

where $|\Psi_0(t)\rangle$ is a time-dependent Slater determinant, to be determined variationally, and $\mathcal{P}_i(x_i, t)$ a time-dependent electron operator at site i that depends explicitly on the phonon coordinate x_i . We define, neglecting the index i for convenience,

$$\mathcal{P} = \sqrt{2} \phi_0(x, t) |0\rangle\langle 0| + \sqrt{2} \phi_1(x, t) (|\uparrow\rangle\langle \uparrow| + |\downarrow\rangle\langle \downarrow|) + \sqrt{2} \phi_2(x, t) |2\rangle\langle 2|, \quad (2)$$

where $\phi_n(x, t)$ are site-dependent phonon wave functions and $|\Gamma\rangle\langle \Gamma|$ is the projector onto the site being empty $\Gamma = 0$, singly occupied by a spin up $\Gamma = \uparrow$, or down $\Gamma = \downarrow$ electron, or, finally, doubly occupied $\Gamma = 2$. Particle-hole symmetry implies that under $n \rightarrow 2 - n$, $\phi_n(x, t) \rightarrow \phi_{2-n}(-x, t)$, namely,

$$\phi_0(x, t) = \phi_2(-x, t), \quad \phi_1(x, t) = \phi_1(-x, t).$$

We evaluate average values on the wave function (1) by means of the Gutzwiller approximation, following Refs. 34 and 32, which amounts to impose that

$$\int dx |\phi_0(x, t)|^2 + |\phi_1(x, t)|^2 = 1.$$

The above condition implies that the average over the Slater determinant $|\Psi_0(t)\rangle$ and the phonons of the operator that remains after extracting from $\mathcal{P}_i(x_i, t)^\dagger \mathcal{P}_i(x_i, t)$ any two fermionic operators vanishes identically. This property allows to evaluate explicitly all average values on the wave function (1) in the limit of infinite lattice coordination,^{34,35} although it is common to use the same results also for lattices with finite coordination numbers, hence the name Gutzwiller approximation.

Within the Gutzwiller approximation, the average value of the Hamiltonian (1) on the wave function $|\Psi(t)\rangle$ can be shown

to coincide with the average on $|\Psi_0(t)\rangle$ of the Hamiltonian

$$\begin{aligned} H_*(t) = & -t \sum_{\langle ij \rangle \sigma} R_i(t) R_j(t) (c_{i\sigma}^\dagger c_{j\sigma} + \text{H.c.}) \\ & + \frac{1}{2} \sum_i \int dx (U + 2gx) |\phi_{0i}(x, t)|^2 \\ & + \frac{\omega}{2} \sum_i \sum_{n=0,1} \int dx \phi_{ni}(x, t)^* h(x) \phi_{ni}(x, t), \end{aligned} \quad (3)$$

where $h(x) = (-\partial_x^2 + x^2)$. The parameters

$$R_i(t) = \int dx [\phi_{1i}(x, t)^* \phi_{0i}(x, t) + \text{c.c.}], \quad (4)$$

are commonly interpreted as the amplitudes of quasiparticles at sites i , hence H_* as their effective noninteracting Hamiltonian with renormalized hopping $t_{ij}(t) \equiv R_i(t) R_j(t) t$.

The variational principle that we assume is the saddle point of the action $\mathcal{S} = \int dt \mathcal{L}(t)$, i.e., $\delta \mathcal{S} = 0$, whose Lagrangian is

$$\mathcal{L}(t) = i \langle \Psi(t) | \dot{\Psi}(t) \rangle - \langle \Psi(t) | H | \Psi(t) \rangle, \quad (5)$$

which, within the Gutzwiller approximation,²⁵ reads simply

$$\begin{aligned} \mathcal{L}(t) = & i \sum_i \sum_{n=0,1} \int dx \phi_{ni}(x, t)^* \dot{\phi}_{ni}(x, t) \\ & + i \langle \Psi_0(t) | \dot{\Psi}_0(t) \rangle - \langle \Psi_0(t) | H_*(t) | \Psi_0(t) \rangle. \end{aligned} \quad (6)$$

We define on each site i a normalized two-component spinor

$$|\Phi_i\rangle = \Phi_i(x_i) \equiv \begin{pmatrix} \phi_{1i}(x_i) \\ \phi_{0i}(x_i) \end{pmatrix}, \quad (7)$$

so that

$$\langle \Phi_i | (\dots) | \Phi_i \rangle = \int dx \Phi_i(x)^\dagger (\dots) \Phi_i(x)$$

and further introduce Pauli matrices σ^a , $a = x, y, z$, which act on the two components of the spinor. With the above notations, the saddle point equations read

$$\begin{aligned} i|\dot{\Phi}_i\rangle = & \frac{\omega}{2} h(x) |\Phi_i\rangle - t \sum_j^{\text{n.n. of } i} R_j w_{ij} \sigma^x |\Phi_i\rangle \\ & + \frac{1}{4} (U + 2gx) (1 - \sigma^z) |\Phi_i\rangle, \end{aligned} \quad (8)$$

$$i|\dot{\Psi}_0\rangle = H_* |\Psi_0\rangle, \quad (9)$$

where

$$R_i = \langle \Phi_i | \sigma^x | \Phi_i \rangle, \quad (10)$$

$$w_{ij} = \sum_\sigma \langle \Psi_0 | (c_{i\sigma}^\dagger c_{j\sigma} + \text{H.c.}) | \Psi_0 \rangle. \quad (11)$$

It is worth noticing here that, when the electron-phonon interaction vanishes, the two subsystems decouple and the above dynamics reduces, for the electronic degrees of freedom, to the one studied in Ref. 24 for the simple Hubbard model. In the general case, one has to integrate the equations of motion starting from initial values for the spinor wave functions and the Slater determinant. In order to integrate the spinor part, we follow the approach outlined in Ref. 32 and project each component on the basis of eigenfunctions of the harmonic

oscillator, the Hermite functions $\varphi_n(x)$, namely, we write for $\nu = 0, 1$,

$$\phi_\nu(x, t) = \sum_{n=0}^{\infty} c_n^\nu(t) \varphi_n(x) \quad (12)$$

and obtain time-dependent equations for the complex coefficients $c_n^\nu(t)$ by plugging this expansion into Eq. (8). In practice, we truncate the basis set to a finite number of coefficients $n = 0, \dots, N_b$ and check that convergence is guaranteed by choosing $N_b \simeq 60$. All calculations that are presented here have been performed on a cubic lattice using $U = 12t$ and the phonon frequency $\omega = t$. An important scale of energy is the value of the critical U_c at the equilibrium Mott transition in the absence of phonons. In the cubic lattice and within the Gutzwiller approximation $U_c = 16t$, whose inverse we shall use as the unit of time. As we mentioned, the Eqs. (8)–(11) are strictly valid only in lattices with infinite coordination numbers, therefore our use in a cubic lattice is just an approximation.

A. The Gutzwiller approximation as a mean-field theory

Equations (9) and (8) resemble time-dependent mean-field equations, with the Schrödinger-like evolution of $|\Psi_0\rangle$ that depends implicitly on the average values of selected operators over the wave functions $|\Phi_i\rangle$, and vice versa for the latter ones. Indeed, one recognizes readily that, given the Hamiltonian

$$\begin{aligned} H_I = & -t \sum_{(ij)\sigma} \sigma_i^x \sigma_j^x (c_{i\sigma}^\dagger c_{j\sigma} + \text{H.c.}) \\ & + \frac{1}{4} \sum_i (U + 2gx_i) (1 - \sigma_i^z) + \frac{\omega}{2} \sum_i (p_i^2 + x_i^2), \end{aligned} \quad (13)$$

where σ_i^a , $a = x, y, z$, are Ising variables defined on each site i , and assuming a factorized wave function

$$|\Psi_I\rangle = |\text{Ising+phonons}\rangle \times |\text{electrons}\rangle, \quad (14)$$

where

$$|\text{Ising+phonons}\rangle = \prod_i |\text{Ising+phonons}\rangle_i,$$

the same variational principle $\delta S = 0$ that we applied before would lead right to Eqs. (9) and (8). The Hamiltonian (13) thus extends to the Hubbard-Holstein model the mapping derived in Ref. 25 for the simple Hubbard model. We just recall that the mapping states that, if Z is the partition function of the original model with the Hamiltonian H of Eq. (1), and Z_I that one of the Hamiltonian H_I of Eq. (13), then, in the limit of infinite coordination lattices and at particle-hole symmetry,

$$Z = \left(\frac{1}{2}\right)^N Z_I, \quad (15)$$

where N is the number of sites.²⁵ Essentially, the mapping demonstrates that the constraint required to implement the so-called slave-spin representation of the Hubbard model^{36–38} is actually unessential in the limit of infinite lattice-coordination and at particle-hole symmetry. The advantage of dealing with H_I instead of the original Hamiltonian is that it provides a

simple framework to disentangle already at the mean-field level the quasiparticle degrees of freedom, the fermionic operators, from the Hubbard bands, the Ising variables.

The chosen factorization (14), where the phonon degrees of freedom are entangled with the Hubbard bands and both influence in a mean-field fashion the quasiparticles, is actually inspired by the DMFT result that, for large repulsion and weak electron-phonon coupling, phonon signatures are hardly visible in the quasiparticle spectrum but quite evident in the Hubbard bands.³⁹ Different choices could be more appropriate in different contexts or easier to deal with, as the extreme factorization $|\Psi_I\rangle = |\text{Ising}\rangle \times |\text{phonons}\rangle \times |\text{electrons}\rangle$.

III. RESULTS

We shall now analyze the time-dependent mean-field equations (9) and (8) that describe within t-GA the evolution of a variational wave function under the action of the Hubbard-Holstein Hamiltonian, or equivalently the Hamiltonian (13).

We will assume that the pump that drives the system out of equilibrium is selective in the sense that it only injects energy in the Hubbard bands, i.e., in the Ising subsystem, specifically increasing the concentration of doubly occupied sites (doublons), hence of empty sites (holons) because of particle conservation. In the Ising language, it corresponds to assuming that initially the average values of σ_i^z are lower than those at equilibrium. We note that the equilibrium conditions are obtained by replacing the time-dependent mean-field equations (9) and (8) with stationary mean-field equations. In particular, the equilibrium values of $|\Phi_i\rangle$ are the lowest energy eigenstates of the right-hand side of Eq. (8), which must be self-consistently determined since the effective Hamiltonian depends on $R_j = \langle \Phi_j | \sigma^x | \Phi_j \rangle$.⁴⁰

As we mentioned earlier, in real experiments the light pulse couples via the vector potential to both Hubbard bands and quasiparticles. Therefore the above assumption is only an approximation, whose validity we intend to weight up in the near future, while, in the present work, we shall keep assuming that the initial state is just characterized by an out-of-equilibrium equal population of doublons and holons. We will consider first the case in which such a population is uniformly distributed over the whole sample and next move to inhomogeneous situations.

A. Whole bulk driven out of equilibrium

Let us therefore consider the Hubbard-Holstein Hamiltonian (1) at half-filling and assume that the system is initially prepared with a uniform concentration of doublons and holons higher than at equilibrium. The system is then let evolve, its time evolution being approximated within t-GA by Eqs. (9) and (8). This case is actually similar to the quench described in Ref. 24; the new ingredient being just the electron-phonon coupling.

We first need to determine the equilibrium condition in the presence of the electron-phonon coupling. This is accomplished by a self-consistent iterative mapping method similar to the one described in Ref. 41. The outcome is a homogeneous wave function, with the same spinor at any site, and the Slater determinant that is just the uniform ground state of the hopping energy. The concentrations of doublons and

holons are then artificially augmented by the same amount, while keeping the phonon wave-function unaltered. This is accomplished by the scale transformation $\phi_0(x) \rightarrow \lambda_0 \phi_0(x)$ and $\phi_1(x) \rightarrow \lambda_1 \phi_1(x)$, with $\lambda_0 > 1$ and $\lambda_1 < 1$ such that normalization is maintained,

$$\int dx \lambda_0^2 |\phi_0(x)|^2 + \lambda_1^2 |\phi_1(x)|^2 = 1,$$

but the concentration of doubly occupied and empty sites is increased. The system is then allowed to evolve as previously explained. The novelty with respect to Ref. 24 is that we can now monitor how the energy, initially injected in the electron subsystem only, is transferred to phonons. We note that because translational symmetry is preserved by the time evolution, the effective Hamiltonian $H_*(t)$ in Eq. (3) has $R_i(t) = R_j(t) = R(t)$, $\forall i, j$, hence describes at all times a simple tight-binding model with uniform time-dependent nearest-neighbor hopping. As a result, the Slater determinant that is initially the lowest energy eigenstate of the hopping, does not change in time, hence cannot provide dissipative channels for the spinor evolution. For this reason, the dynamics of both electronic and phononic observables lack relaxation to a steady state but rather shows undamped coherent oscillations. Still, as shown in Ref. 24, the mean-field dynamics captures important features of the nonequilibrium problem and provides a qualitatively correct picture of the short-to-intermediate time dynamics.

In Fig. 1, we plot the time evolution of the renormalization factor $R_i(t) = R(t)$, Eq. (10), which shows two distinct regimes of oscillations depending on the amount of doublons injected, δD , which measures the strength of the nonequilibrium perturbation and that we define as $\delta D \equiv D(t=0) - D_{\text{eq}}$, with $D(t=0)$ the initial value and D_{eq} the equilibrium one.

For small perturbations, R oscillates around a finite average, while, upon increasing δD above a threshold, it oscillates from -1 to $+1$, with average zero. In the Ising model language of Sec. II A, this behavior is representative of the transition from the ordered phase, $\langle \sigma^x \rangle \neq 0$, to the disordered one, $\langle \sigma^x \rangle = 0$. A similar dynamical transition was observed in Ref. 24 for the pure Hubbard model without electron-phonon coupling. The mean-field coherent oscillations, although artificial, reflect the real tendency of the system to be trapped into long-lived prethermal metastable states whose properties are correctly

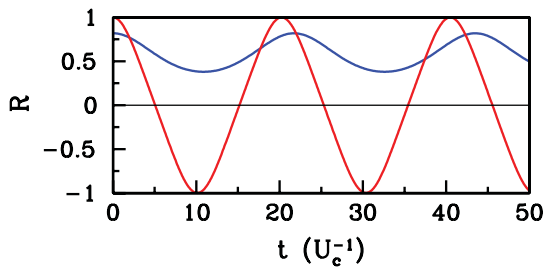


FIG. 1. (Color online) The time evolution of the parameter $R_i = R$, Eq. (10) for two different concentrations δD of injected doublons, one below and the other above the critical point, see Fig. 2. Below the critical point, $\delta D = 4\%$ (blue curve), R oscillates around a finite value, while, above, $\delta D = 17\%$ (red curve), it oscillates between $+1$ and -1 with zero average.

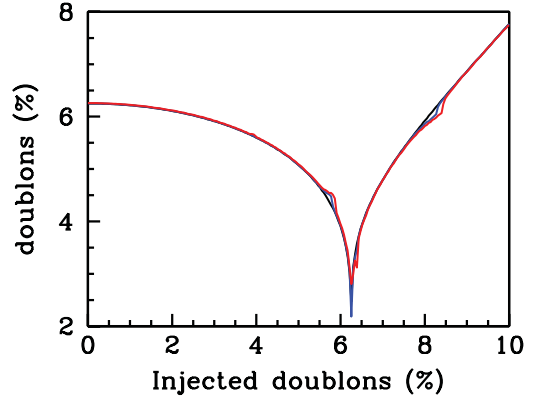


FIG. 2. (Color online) The time average value of the percentage of doubly occupied sites as a function of the percentage δD of doublons, hence holons, injected in the initial state with respect to the equilibrium value. We plot three values of the electron-phonon couplings, $g = 0$ (black), $g = 0.1t$ (blue), and $g = 0.2t$ (red). Larger g correspond to more pronounced kinks near the critical point, which is identified by the point at which the double occupancy drops down.

captured by the long-time averages of the mean-field dynamics.

With this insight, we plot in Fig. 2 the time-averaged double occupancy as a function of the concentration of injected doublons δD . The first observation is that the electron-phonon interaction does not change qualitatively the behavior with respect to the Hubbard model alone, see Ref. 24; namely, we still find two distinct regimes separated by a critical point where the double occupancy goes to zero, although numerically we cannot hit the precise value when this occurs. We note that the location of the critical point is not appreciably affected by phonons because of the tiny electron-phonon coupling ($g^2/\omega \sim 10^{-3} U$).

We find that the transition occurs right when the initial energy happens to coincide with the equilibrium energy at the Mott transition,^{24,31} which is simply the zero-point energy of the phonons for our model Hamiltonian (1) and within the Gutzwiller approximation. In fact, one readily realizes that Eqs. (8) and (9) admit another stationary point besides the one that corresponds to the equilibrium condition, namely, $\phi_0(x) = 0$ hence $R = 0$, with energy just $\omega/2$. We finally mention that, unlike in the absence of phonons,²⁴ here the critical point is not associated to an exponential relaxation toward a stationary state that seems to be a characteristic of integrable dynamics,³¹ which is presumably not our case.

We now move our attention to the phonon sector, in order to unveil the entanglement between the electrons and the lattice as the former are driven out of equilibrium. A natural quantity to look at would be the average lattice displacement $\langle x_i \rangle$, which, however, is constrained to be zero on average by particle-hole symmetry. Still, we can define as a measure of the effective displacement the average of the operator $q_i \equiv x_i(n_i - 1)$, which is just the electron-phonon coupling operator. In Fig. 3, we plot the relative variation of the time-averaged effective displacement

$$q_* = \lim_{\tau \rightarrow \infty} \frac{1}{\tau} \int_0^\tau dt \langle q_i(t) \rangle, \quad (16)$$

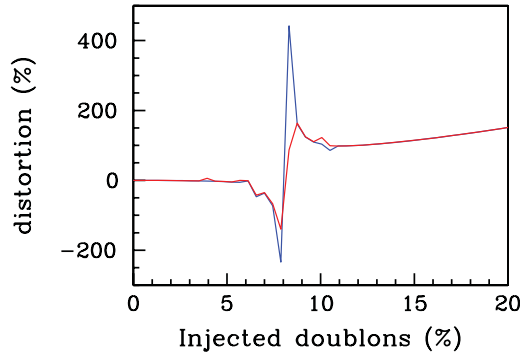


FIG. 3. (Color online) The time average value of the lattice distortion, defined as the relative variation with respect to the equilibrium value, as function of the percentage of doublons δD injected in the initial state with respect to the equilibrium value. The curve that is more singular near the critical point corresponds to $g = 0.1t$ (blue), the other to $g = 0.2t$ (red).

i.e., $(q_* - q_{\text{eq}})/q_{\text{eq}}$, where q_{eq} is the equilibrium value, as a function of the concentration of injected doublons. We note that, at small concentrations, the displacement is mostly unchanged from its equilibrium value. However, for higher concentrations past the critical point, the displacement starts increasing substantially; a growing distortion being a way to store the initial excess energy.

Although the gross behavior seems not to be affected by phonons, there are details that feature their presence. In particular, we note some anomalies, tinier in Fig. 2 and more visible in Fig. 3. These anomalies appear when the oscillation frequency of the electronic dynamics, which decreases on approaching the critical point, hits the renormalized phonon frequency, or a multiple of it. Since the latter is small, these resonances occur near the critical point. This is evident in Fig. 4, where we draw by a color plot the spectral decomposition of the time evolutions both of the double occupancy and the phonon distortion as a function of the concentration of injected doublons and of the frequency of the signal. In particular, we observe the avoided crossing between the two lowest frequencies around $\delta D \sim 5\%$ that causes the kink visible in Fig. 2. Among these two frequencies, the lowest one is visible mostly in the dynamics of $q(t)$, hence

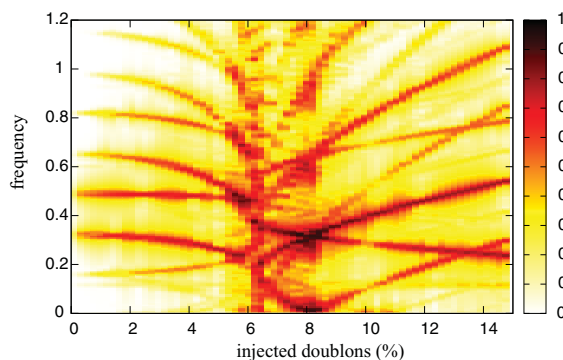


FIG. 4. (Color online) Color plot of the Fourier transform (in arbitrary units) of the time evolutions of the double occupancy and the effective phonon distortion, as a function of the concentration of injected doublons and of the frequency in units of U_c .

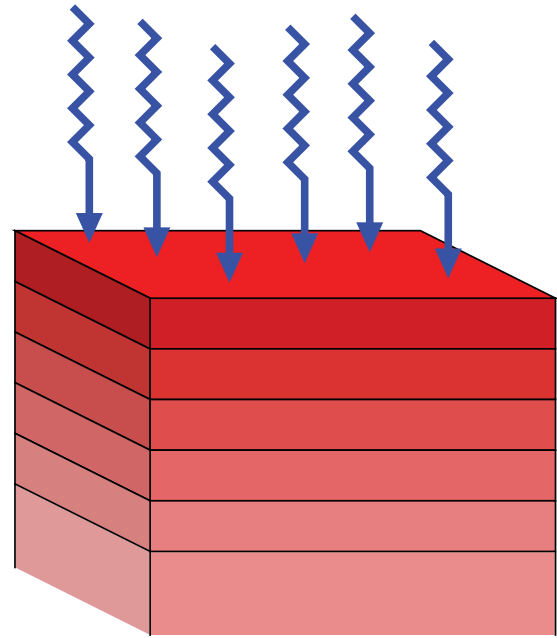


FIG. 5. (Color online) Slab geometry for simulating the hypothetical experiment in which only the surface layer is driven out of equilibrium.

can be regarded as a renormalized phonon frequency that blue shifts upon increasing δD , i.e., the energy injected into the system. As we mentioned, the transition point in this case is not associated to a simple exponential relaxation as in the absence of phonons.²⁴ This is evident in the Fourier spectrum of Fig. 4, which shows that the time signal is characterized by many different oscillatory components also nearby the transition, thus preventing us from identifying unambiguously a diverging time scale. However, the observation that the transition is associated, in the Ising language, to a dynamical order-to-disorder transition, suggests that such a time scale should exist, even though we are unable to extract it.

B. Surface driven out of equilibrium

Let us now consider a slab geometry as depicted in Fig. 5, denoting by z the direction perpendicular to the surface, which lies in the xy plane. This setting allows us to mimic the nonequilibrium dynamics across a correlated heterostructure that has recently attracted experimental interest.²⁹ We consider a system described by the Hubbard-Holstein model and consider a perturbation acting only at the surface layer by triggering an out-of-equilibrium population of doublons and holons, while keeping the bulk in its equilibrium ground-state configuration. This initial state is then let evolve and its time evolution is approximated by the Eqs. (9) and (8).

This particular geometry has the additional complication that, at equilibrium, the optimized $|\Phi_i\rangle$ are layer dependent and the optimized Slater determinant is not uniform anymore. Therefore the first step we need to undertake is solving the equilibrium problem, which we accomplish by the method developed in Ref. 41. Because of the slab geometry, we can choose a basis of single-particle wave functions for building

the Slater determinant defined by

$$\psi_{\epsilon\mathbf{k}}(\mathbf{r}, i) = \frac{e^{i\mathbf{k}\cdot\mathbf{r}}}{\sqrt{A}} \psi_{\epsilon\mathbf{k}}(i),$$

where \mathbf{r} is the space coordinate and $\mathbf{k} = (k_x, k_y)$ the momentum in the xy plane, which is assumed to contain A lattice sites, while $i = 1, \dots, N$ is the layer index, and typically, we used $N = 100$ layers. Since there is translational symmetry in the xy plane, we can choose the spinor $|\Phi_i\rangle$ to depend only on the layer index i . Then, the stationary solution of Eqs. (8) and (9) amounts to solve at fixed R_i the eigenvalue problem

$$\epsilon \psi_{\epsilon\mathbf{k}}(i) = t R_i^2 \epsilon_{\mathbf{k}} \psi_{\epsilon\mathbf{k}}(i) - t R_i \sum_{a=\pm 1} R_{i+a} \psi_{\epsilon\mathbf{k}}(i+a), \quad (17)$$

where $\epsilon_{\mathbf{k}} = -2(\cos k_x + \cos k_y)$ with the boundary condition $\psi_{\epsilon\mathbf{k}}(0) = \psi_{\epsilon\mathbf{k}}(N+1) = 0$. The lowest energy eigenfunctions $\epsilon < \epsilon_F$, $\epsilon_F = 0$ because of particle-hole symmetry, are then used to define the Slater determinant $|\Psi_0\rangle$ and the average hopping between layer i and $i+a$,

$$w_{i \rightarrow i+a} = \frac{1}{A} \sum_{\epsilon < 0} \sum_{\mathbf{k} \ni \epsilon < 0} [\psi_{\epsilon\mathbf{k}}(i)^* \psi_{\epsilon\mathbf{k}}(i+a) + \text{c.c.}], \quad (18)$$

as well as the average hopping within layer i ,

$$w_{i \rightarrow i} = \frac{1}{A} \sum_{\epsilon < 0} \sum_{\mathbf{k} \ni \epsilon < 0} \epsilon_{\mathbf{k}} |\psi_{\epsilon\mathbf{k}}(i)|^2. \quad (19)$$

These parameters are used to solve the spinor eigenvalue problem

$$\begin{aligned} E|\Phi_i\rangle &= \frac{\omega}{2} h(x)|\Phi_i\rangle - t R_i w_{i \rightarrow i} \sigma^x |\Phi_i\rangle \\ &\quad - t \sum_{a=\pm 1} R_{i+a} w_{i \rightarrow i+a} \sigma^x |\Phi_{i+a}\rangle \\ &\quad + \frac{1}{4}(U + 2gx)(1 - \sigma^z)|\Phi_i\rangle, \end{aligned} \quad (20)$$

whose lowest energy solution defines new parameters $R_i = \langle \Phi_i | \sigma^x | \Phi_i \rangle$ that are used to solve again Eq. (17) and so on, until convergence is reached.^{40,41}

The breaking of translational symmetry by the presence of the surfaces is actually amplified by electron correlations that create a surface dead layer,^{41,42} with suppressed double occupancy, hence reduced hopping renormalization parameters R_i . The dead layer penetrates inside the bulk over a length proportional to the Mott-transition correlation length.^{41,42}

Given this starting state, we suddenly increase the population of doublons and holons on the first layer $i = 1$ and let the system evolve. Essentially, we simply turn Eqs. (17) and (20) into self-consistent nonlinear time-dependent Schrödinger equations that we solve numerically. Unlike in the homogeneous case of Sec. III A, here the Slater determinant evolves with time because the wave functions $\psi_{\epsilon\mathbf{k}}(i, t)$ acquire a non-trivial time dependence, which provides additional dissipative channels that were previously absent. In other words, the hopping parameters $w_{i \rightarrow i+a}(t)$ and $w_{i \rightarrow i}(t)$ defined in Eqs. (18) and (19) become time-dependent and influence the evolution of $|\Phi_i\rangle$, see Eq. (20), which in turns affects $\psi_{\epsilon\mathbf{k}}(i, t)$ via the parameters $R_i(t)$.

The mutual feedback between $|\Psi_0\rangle$ and the $|\Phi_i\rangle$'s brings about a nontrivial dynamics much richer than in the example

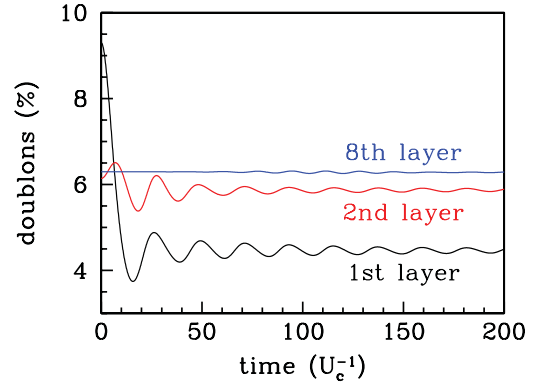


FIG. 6. (Color online) Time evolution of the percentage of doubly occupied sites on three different layers, indicated in the figure, for small percentage of injected doublons. The time is measured in units of the inverse of U_c . The simulation is performed with a slab of 100 layers.

discussed in Sec. III A. Nevertheless, even in this case, we do find two completely different dynamical behaviors, depending on the amount of injected doublons.

For small values, the perturbed surface layer is able to relax by dissipating its excess energy inside the bulk, see Fig. 6. Indeed, the time-average values of the double occupancies on each layer tend toward their equilibrium values, which, as we mentioned, are lower the closer the layer to the surface. We emphasize that here, as opposed to the previous case and to the case of global quantum quenches, the perturbation is local and the energy injected does not scale with the system size. As a result, the relaxation dynamics we find in this regime is toward the equilibrium ground state and no heating or finite-temperature effects are expected in the long-time limit. This is a specific example of a local quantum quench and shows that our time-dependent Gutzwiller approximation, with the above mentioned feedback between variational parameters and Slater determinant, is able to describe thermalization. We also mention that, working with a finite-size geometry, recurrence effects are present at long enough times, when the perturbation reaches the opposite surface and starts oscillating back and forth. In particular, we find that the perturbation propagates ballistically with a large speed that seems to be controlled by the bare value of the hopping. For this reason, we cannot really reach the equilibrium state, which would be, e.g., signaled by the second layer double occupancy in Fig. 6 reaching the same value as at the initial time $t = 0$, because the perturbation hits the opposite end of the slab before equilibration sets in. We expect that by taking the thermodynamic limit in the z direction, these finite-size effects will be washed away. Nevertheless, even for finite lengths the relaxation and the trend toward equilibrium are clearly evident.

Upon increasing the concentration of injected doublons a different dynamical behavior emerges. In particular, above a certain threshold, the excitation remains trapped near the surface, see Fig. 7. This is quite remarkable because, as we mentioned, the Slater determinant now adjusts to the spinors $|\Phi_i\rangle$ during the time evolution, hence could, in principle, absorb the excess energy and transfer it in the interior of the bulk. What actually happens is that the parameters R_i and

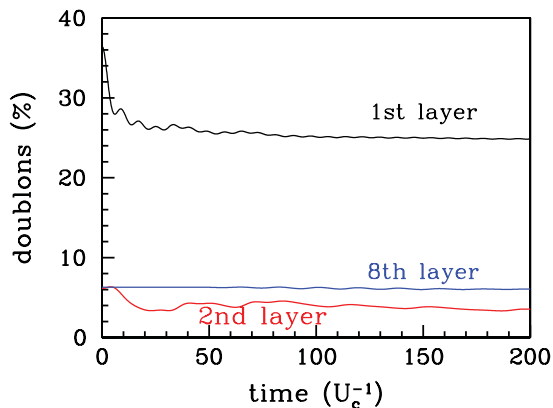


FIG. 7. (Color online) Same as Fig. 6 at higher percentage of injected doublons.

R_{i+1} of adjacent layers interfere destructively, i.e., oscillate out of phase, at some i near the surface, effectively suppressing the quasiparticle interlayer hopping $t_{ii+1} = R_i R_{i+1} t$, hence cutting layer i from the rest of the bulk. In the particular case that Fig. 7 refers to, it is actually the first layer, $i = 1$, that decouples from the rest of the slab, a consequence of having injected energy only in such a layer that already at equilibrium is poorly connected to the bulk. In the Ising language of Sec. II A, this behavior is easier to comprehend. Essentially, the Ising order parameter $R_1 = \langle \sigma_1^x \rangle$ starts to oscillate between $+1$ and -1 with vanishing average, signaling that layer 1 is driven into the symmetric phase. The order parameter of layer 2, $R_2 = \langle \sigma_2^x \rangle$, also oscillates but around a small yet finite value. However, because the oscillations are not synchronized, $R_1 \cdot R_2$ averages to zero; the first layer decouples effectively from the second. This anomalous trapping exists also in the absence of electron-phonon coupling, hence it is primarily an electronic effect, presumably the dynamical counterpart of the surface dead layer at equilibrium.^{41,42} What changes at finite electron-phonon coupling is that this phenomenon is accompanied by a lattice deformation, also localized on the uppermost layers, see Fig. 8.

The physical picture that emerges can be visualized much better by the long-time layer-dependent profiles of the percentages of doubly occupied sites and of the distortion, shown in Fig. 9. We observe that the deviations of both quantities

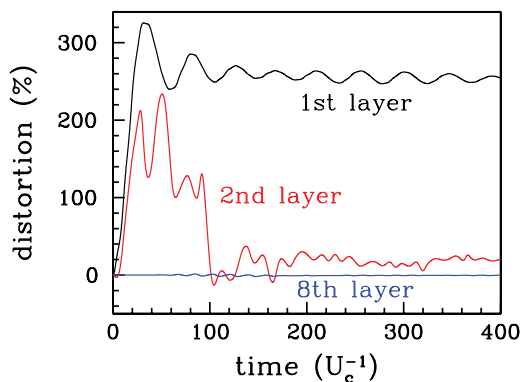


FIG. 8. (Color online) The lattice distortion on three different layers with the same amount of injected doublons as in Fig. 7.

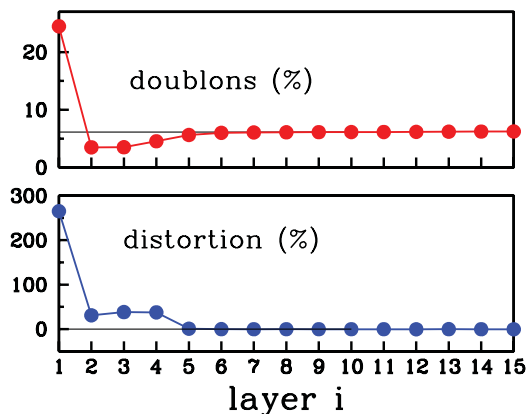


FIG. 9. (Color online) The percentage of doubly occupied sites and of the lattice distortion at each layer at very long times.

with respect to equilibrium are indeed concentrated just near the surface, while the bulk is practically unaffected. Also instructive are the profiles of the intralayer and interlayer hopping renormalization factors, R_i^2 and $R_i R_{i+1}$, shown in Fig. 10. We note that the first layer has a much larger hopping renormalization factor R_1^2 than at equilibrium, when it would be very small due to the dead layer phenomenon.^{41,42} However, this layer is practically decoupled from the second layer, $R_1 R_2$ being vanishingly small.

We end by mentioning that, in contrast to the case of Sec. III A, the two different regimes that we observe seem not to be separated by a genuine dynamical critical point, but rather by the dynamical counterpart of a first-order phase transition. Indeed, in the intermediate regime, the system does not show a well defined behavior but instead oscillates between the two distinct phases above. Right for the same reason, we cannot state that the change of behavior occurs when the energy stored in the first layer is that of a Mott insulating layer. However, what we can definitely state, especially in view of the Ising analogy of Sec. II A, is that what we observe is a genuine surface dynamical-phase transition, presumably first order as far as we can judge.

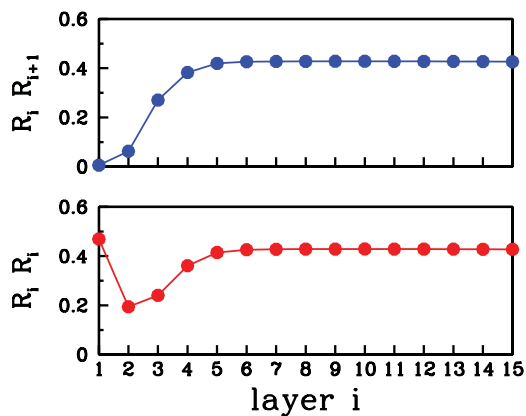


FIG. 10. (Color online) The intralayer, bottom panel, and interlayer, top panel, hopping renormalization factors at long times.

IV. CONCLUSIONS

In this work, we have studied the real time dynamics of the Hubbard-Holstein model at half-filling by a very simple extension of the Gutzwiller approximation in two different toy cases: (i) a bulk system is prepared with an equal out-of-equilibrium population of doubly occupied and empty sites and let evolve in time, and (ii) a slab is considered and it is assumed that only the surface layer is initially driven out of equilibrium.

In case (i), we find similar results as in the quantum quench of the pure Hubbard model: a dynamical critical point that separates two different regimes. The novel feature introduced by the phonons is the presence of a substantial phonon displacement that occurs for large enough deviation from equilibrium, a remarkable outcome in that the electron-phonon coupling we consider is extremely small as compared with the Hubbard repulsion.

In the slab geometry (ii), we still find two dynamical behaviors, although this time without a true dynamical transition in between. If the energy injected at the surface is below a threshold, it is able to flow within the bulk and the system seems to relax toward the equilibrium ground state with the dead layer near the surface.^{41,42} On the contrary, if the excess energy at the surface exceeds that threshold, it does not succeed anymore to flow in the bulk and remains concentrated practically at the surface, bringing about a substantial phonon displacement. Surprisingly, we find that the first layer has a larger hopping renormalization factor than at equilibrium, which can be sustained because the layer effectively decouples from the rest of the system. However, we can not conclude that such an enhancement corresponds to an increased metallicity, which would be indeed a remarkable result. In fact, we tend to believe that the hopping renormalization as defined within the Gutzwiller approximation is a measure of the whole, coherent plus incoherent, single-particle spectrum at low energy, not just of the quasiparticle coherent contribution alone. Therefore, what we feel safe to state is just that the low-energy spectral weight grows in the first layer, whatever being its nature.

We cannot exclude that such a long-lived localized excitation could indeed correspond to some kind of exciton already

present in the equilibrium spectrum, which can be unveiled by our variational technique only because we are exploring the dynamics. It is also plausible that such a localized excitation exists just in correspondence with the surface dead layer,^{41,42} where the low-energy spectral weight is negligible hence there is room for excitons inside the preformed Mott-Hubbard gap. Indeed, if we repeat the calculation by pumping energy on a layer inside the slab, we do find a similar behavior but for much higher values of the concentration of injected doublons. Therefore we tend to believe that, should a Mott exciton exist, it would be more likely visible on the surface dead layer. It is as well possible that our finding is actually related to the debated issue about the lifetime of doublons in the strongly interacting Hubbard model,^{9,22,43} which could also be the clue to understand the lack of thermalization of highly excited states when correlation is strong. Further investigations with different and complementary approaches are needed to clarify these interesting issues.

Finally, we think it is worth discussing how it could be possible to detect experimentally such a surface trapping. In principle, for a laser pump with grazing incidence, only the first uppermost surface layers are effectively excited. If the fluence is high so that the injected energy per unit area is large enough, it could be possible to drive the surface layers sufficiently far from equilibrium to observe the phenomenon. In this case, we expect that more than a single layer should be involved. Nevertheless, if the incident angle between the probe beam and the surface can be varied, one could discriminate between the response of the surface layers and the bulk ones, hence observe what we predict.

ACKNOWLEDGMENTS

This work has been supported by the European Union, Seventh Framework Programme, under the project GO FAST, grant agreement No. 280555. M.F. also thanks Marino Marsi for useful discussions and the hospitality of the Laboratoire de Physique des Solides, Université Paris-Sud, Orsay (France), where this work was completed.

¹G. Giannetti *et al.*, *Nat. Communication* **2**, 353 (2011).

²H. Ichikawa *et al.*, *Nat. Mater.* **10**, 101 (2010).

³D. Fausti, R. I. Tobey, N. Dean, S. Kaiser, A. Dienst, M. C. Hoffmann, S. Pyon, T. Takayama, H. Takagi, and A. Cavalleri, *Science* **331**, 189 (2011).

⁴N. Dean, J. C. Petersen, D. Fausti, R. I. Tobey, S. Kaiser, L. V. Gasparov, H. Berger, and A. Cavalleri, *Phys. Rev. Lett.* **106**, 016401 (2011).

⁵M. Eckstein and M. Kollar, *Phys. Rev. B* **78**, 205119 (2008).

⁶M. Eckstein and M. Kollar, *Phys. Rev. B* **78**, 245113 (2008).

⁷J. K. Freericks, H. R. Krishnamurthy, and T. Pruschke, *Phys. Rev. Lett.* **102**, 136401 (2009).

⁸B. Moritz, T. P. Devereaux, and J. K. Freericks, *Phys. Rev. B* **81**, 165112 (2010).

⁹M. Eckstein and P. Werner, *Phys. Rev. B* **84**, 035122 (2011).

¹⁰W. H. Parker, *Phys. Rev. B* **12**, 3667 (1975).

¹¹P. B. Allen, *Phys. Rev. Lett.* **59**, 1460 (1987).

¹²L. Perfetti, P. A. Loukakos, M. Lisowski, U. Bovensiepen, H. Berger, S. Biermann, P. S. Cornaglia, A. Georges, and M. Wolf, *Phys. Rev. Lett.* **97**, 067402 (2006).

¹³J. Tao and J.-X. Zhu, *Phys. Rev. B* **81**, 224506 (2010).

¹⁴D. B. McWhan and J. P. Remeika, *Phys. Rev. B* **2**, 3734 (1970).

¹⁵F. J. Morin, *Phys. Rev. Lett.* **3**, 34 (1959).

¹⁶*Colossal Magnetoresistive Manganites*, edited by T. Chatterji (Kluwer Academic, Dordrecht, 2004).

¹⁷A. Georges, G. Kotliar, W. Krauth, and M. J. Rozenberg, *Rev. Mod. Phys.* **68**, 13 (1996).

¹⁸A. Polkovnikov, K. Sengupta, A. Silva, and M. Vengalattore, *Rev. Mod. Phys.* **83**, 863 (2011).

¹⁹M. Moeckel and S. Kehrein, *Phys. Rev. Lett.* **100**, 175702 (2008).

- ²⁰M. Eckstein, M. Kollar, and P. Werner, *Phys. Rev. Lett.* **103**, 056403 (2009).
- ²¹M. Eckstein, M. Kollar, and P. Werner, *Phys. Rev. B* **81**, 115131 (2010).
- ²²N. Strohmaier, D. Greif, R. Jördens, L. Tarruell, H. Moritz, T. Esslinger, R. Sensarma, D. Pekker, E. Altman, and E. Demler, *Phys. Rev. Lett.* **104**, 080401 (2010).
- ²³G. Carleo, F. Becca, M. Schiró, and M. Fabrizio, *Sci. Rep.* **2**, 243 (2012).
- ²⁴M. Schiró and M. Fabrizio, *Phys. Rev. Lett.* **105**, 076401 (2010).
- ²⁵M. Schiró and M. Fabrizio, *Phys. Rev. B* **83**, 165105 (2011).
- ²⁶M. Först, C. Manzoni, S. Kaiser, T. Tomioka, Y. Tokura, R. Merlin, and A. Cavalleri, *Nat. Phys.* **7**, 854 (2011).
- ²⁷B. Mansart, D. Boschetto, S. Sauvage, A. Rousse, and M. Marsi, *Europhys. Lett.* **92**, 37007 (2010).
- ²⁸B. Mansart, D. Boschetto, A. Savoia, F. Rullier-Albenque, F. Bouquet, E. Papalazarou, A. Forget, D. Colson, A. Rousse, and M. Marsi, *Phys. Rev. B* **82**, 024513 (2010).
- ²⁹A. D. Caviglia *et al.*, e-print [arXiv:1111.3155](https://arxiv.org/abs/1111.3155).
- ³⁰M. S. Foster, E. A. Yuzbashyan, and B. L. Altshuler, *Phys. Rev. Lett.* **105**, 135701 (2010).
- ³¹B. Scioffa and G. Biroli, *J Stat. Mech.* (2011) P11003.
- ³²P. Barone, R. Raimondi, M. Capone, C. Castellani, and M. Fabrizio, *Phys. Rev. B* **77**, 235115 (2008).
- ³³P. Barone, R. Raimondi, M. Capone, C. Castellani, and M. Fabrizio, *Europhys. Lett.* **79**, 47003 (2007).
- ³⁴M. Fabrizio, *Phys. Rev. B* **76**, 165110 (2007).
- ³⁵J. Bünemann, W. Weber, and F. Gebhard, *Phys. Rev. B* **57**, 6896 (1998).
- ³⁶L. de' Medici, A. Georges, and S. Biermann, *Phys. Rev. B* **72**, 205124 (2005).
- ³⁷S. D. Huber and A. Rüegg, *Phys. Rev. Lett.* **102**, 065301 (2009).
- ³⁸A. Rüegg, S. D. Huber, and M. Sigrist, *Phys. Rev. B* **81**, 155118 (2010).
- ³⁹G. Sangiovanni, M. Capone, C. Castellani, and M. Grilli, *Phys. Rev. Lett.* **94**, 026401 (2005).
- ⁴⁰N. Lanatà, H. U. R. Strand, X. Dai, and B. Hellsing, *Phys. Rev. B* **85**, 035133 (2012).
- ⁴¹G. Borghi, M. Fabrizio, and E. Tosatti, *Phys. Rev. Lett.* **102**, 066806 (2009).
- ⁴²F. Rodolakis, B. Mansart, E. Papalazarou, S. Gorovikov, P. Vilmercati, L. Petaccia, A. Goldoni, J. P. Rueff, S. Lupi, P. Metcalf, and M. Marsi, *Phys. Rev. Lett.* **102**, 066805 (2009).
- ⁴³D. Hansen, E. Perepelitsky, and B. S. Shastry, *Phys. Rev. B* **83**, 205134 (2011).